a shift in the isotropic g value and an increase in the observed line width, as shown in Table V.

Conclusions

Single crystals of ion-radical salts of the π-donor TSeN have been obtained for the first time. The 1:1 salts $TSeN^{\bullet+}X^-$ (X = Cl, Br) have isomorphous crystal structures. The structure of $TSeN^{\bullet+}Cl^-$ reveals dimers of parallel cation radicals as well as the changes in molecular geometry that occur on electron loss from TSeN. $TSeN^{\bullet+}Br^-$, an electrical semiconductor, exhibits Curie law paramagnetism in both static susceptibility and electron spin resonance studies. The detailed assessment of the potential of TSeN as a precursor to ion-radical salts with novel solid-state properties requires investigations beyond this initial study, and such research has been initiated.[4]

Supplementary Material Available: Table S-I, presenting experimental details for the structure determination, and Table S-II, listing thermal parameters (3 pages); a table of observed and calculated structure amplitudes (4 pages). Ordering information is given on any current masthead page.

Contribution from the Department of Chemistry, Princeton University, Princeton, New Jersey 08544, Department of Chemistry, Rider College, Lawrenceville, New Jersey 08648, and Department of Physics, Nuclear Research Center, "Demokritos", Athens, Greece

Chloride-Induced Assembly of Manganese(II) Complexes Having Oligomeric and Chain Structures

B. C. Unni Nair,[†] J. E. Sheats,[‡] R. Ponteciello,[‡] D. Van Engen,[†] V. Petrouleas,[§] and G. C. Dismukes*[,†]

Received October 5, 1988

The planar tridentate ligand 2,6-diacetylpyridine dioxime (H_2dapd) forms complexes with Mn(II) having stoichiometries that are determined by the nature of the counterion. The monomeric bis chelate complex $Mn(H_2dapd)_2X_2$ forms with outer-sphere counterions $X = Br^-$ (**3**) and ClO_4^- (**2**). However, with Cl^- a discrete oligomeric complex, $[Mn(H_2dapd)Cl_2]_n$, probably dimeric ($n = 2$) or tetrameric ($n = 4$), forms in nonprotic solvents like DMF, while only a monomeric Mn(II) complex forms in protic solvents. This is in equilibrium with a linear-chain polymer $n = \infty$ (**1**) in the solid state. Compound **1** crystallizes in the monoclinic space group *Cc* [$Z = 4$, $a = 17.843$ (3) Å, $b = 10.422$ (2) Å, $c = 6.809$ (1) Å, $\beta = 106.49$ (0)°]. Mn coordinates to form pentagonal bipyramids $Mn(N_3Cl_2)Cl_2$ in which each chloride occupies axial and equatorial sites on adjacent monomer units in the helical chains. Variable-temperature magnetic susceptibility indicates weak ferromagnetic coupling in **1** ($\mu_{eff} = 8.40\ \mu_B$ at 4.2 K and 6.02 μ_B at 294 K), with an effective spin-exchange temperature of $T_0 = 5$ K ($J = 0.2\ cm^{-1}$), using a one-dimensional linear-chain classical model. This contrasts with the monomeric complex **2**, which exhibits a temperature-independent moment 5.94-5.81 μ_B between 294 and 4.2 K, indicating no intermolecular coupling. The oligomeric complex of **1** in DMF also exhibits ferromagnetic coupling, as seen by the EPR-active paramagnetic ground state. Possible structures are discussed. The weaker ionic bonding between Mn(II) and Br^- and ClO_4^- vs Cl^- accounts for the formation of the bis chelate complexes **2** and **3**. The capacity for Cl^- to spontaneously assemble an oligomeric Mn(II) cluster in solution is compared with the special requirement for Cl^- for assembly of the polynuclear manganese complex responsible for photosynthetic water oxidation.

Introduction

Oximes are well-known chelating agents that form a variety of metal complexes. 2,6-Diacetylpyridine dioxime (H_2dapd) is

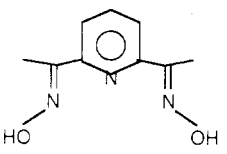

H_2dapd

a particularly interesting planar N,N,N-donor chelating ligand. Fe(II) and Ni(II) form mononuclear complexes with this ligand.[1-3] McCormic et al.[4] have isolated the monomeric, five-coordinate copper complex $[Cu(Hdapd)(Cl)_2]$ and the dimeric dication $[Cu(Hdapd)]_2^{2+}$. Complexes with Mn(II) and H_2dapd have not yet been reported. We were prompted to study the coordination chemistry of this ligand because of the opportunity for formation of discrete Mn aggregates dictated by the incomplete coordination presented by the planar tridentate ligand. Tetrameric and dimeric manganese sites are of biological importance in the enzymes responsible for photosynthetic water oxidation[5] and within the pseudocatalase of *L. planatarum*,[6] respectively. In this study we report the synthesis of manganese(II) complexes with H_2dapd and provide EPR, X-ray crystallographic, and magnetic susceptibility evidence for the special capability of chloride for inducing assembly of an oligomeric Mn(II) complex in aprotic solvents and a linear-chain polymer in the solid state. This is discussed in relation to the chloride requirement observed for photooxidation of the manganese enzyme in photosynthetic water oxidation.

Table I. Crystallographic Data for **1**

chem formula	$C_9H_{11}Cl_2MnN_3O_2$	fw	319.1
a	17.843 (3) Å	space group	*Cc*
b	10.422 (2) Å	T	296 K
c	6.809 (1) Å	λ	0.710 69 Å
β	106.49 (1)°	ρ_{calc}	1.75 g/cm^3
V	1214.1 (4) Å^3	μ	15.7 cm^{-1}
Z	4	trans coeff	0.458-0.552
$R(F_o)$	0.039	$R_w(F_o)$	0.045

Experimental Section

2,6-Diacetylpyridine Dioxime (H_2dapd) ($C_9H_{11}N_3O_2$). The ligand was prepared from hydroxylamine hydrochloride and 2,6-diacetylpyridine by a literature procedure.[7]

$[Mn(H_2dapd)Cl_2]_n$ (1). H_2dapd (0.01 mol) was dissolved in ethanol (50 mL). To this solution was added $MnCl_2 \cdot 4H_2O$ (0.01 mol) and the solution refluxed for 1 h and cooled to form a yellow precipitate. Crystals for X-ray crystallography studies were obtained by slowing boiling off excess ethanol from a dilute solution of the compound. For analysis, the compound was recrystallized from a mixture of ethanol-DMF (1:1). Anal. Calcd for $(C_9H_{11}N_3O_2)MnCl_2$: C, 33.86; H, 3.45; N, 13.17; Mn, 17.25. Found: C, 33.68; H, 3.44; N, 12.71; Mn, 17.75.

[†] Princeton University.
[‡] Rider College.
[§] Nuclear Research Center.

(1) Hanania, G. I. H.; Irvine, D. H.; Shuragh, F. *J. Chem. Soc.* **1965**, 1149.
(2) Bancom, E. I.; Drago, R. S. *J. Am. Chem. Soc.* **1971**, *93*, 6469.
(3) Sproul, G.; Stucky, G. D. *Inorg. Chem.* **1973**, *12*, 2898.
(4) Nicholson, G. A.; Lazarus, C. R.; McCormic, B. J. *Inorg. Chem.* **1980**, *19*, 192.
(5) Dismukes, G. C. *Photochem. Photobiol.* **1986**, *43*, 99-115.
(6) Beyer, W. F., Jr.; Fridovitch, I. *Biochemistry* **1986**, *24*, 6420.
(7) Mohan, M.; Kumar, M. *Synth. React. Inorg. Met. Org. Chem.* **1983**, *13*, 639.

0020-1669/89/1328-1582$01.50/0 © 1989 American Chemical Society

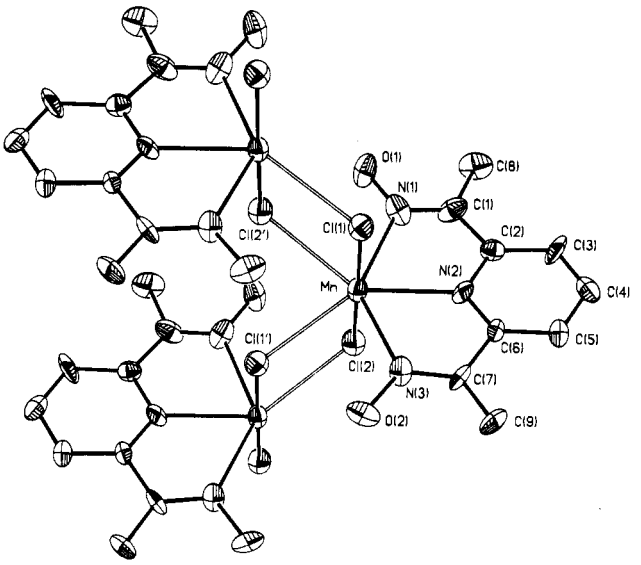

Figure 1. View of the coordination of three monomer units in a single chain.

$[Mn(H_2dapd)_2(X)_2]$. Perchlorate (**2**) and bromo (**3**) derivatives were prepared by the same method as that for the chloride derivative by using 0.01 mol $Mn(ClO_4)_2 \cdot 4H_2O$ and 0.01 mol $MnBr_2$, respectively. The perchlorate derivative (**2**) was recrystallized from a solution of ethanol–DMF (1:1). Anal. Calcd for $(C_9H_{11}N_3O_2)_2Mn(ClO_4)_2$: C, 33.75; H, 3.44; N, 13.13; Mn, 8.59. Found: C, 33.97, H, 3.67; N, 12.92; Mn 8.41. Fw = 640.2. Specific conductivity = 127.6 mho cm^2 mol^{-1} in DMF. Solution magnetic susceptibility = 5.99 μ_B/Mn at room temperature in DMF.

Spectroscopy. Infrared spectra of the compounds were run as KBr disks. EPR spectra were recorded on frozen solutions of the complexes in dimethylformamide (DMF) or CH_3CN (**2**, **3**) at X-band frequency by using a Varian E-12 spectrometer and an Oxford helium cryostat. Magnetic susceptibility measurements were carried out on solutions at room temperature by using the Evans method.[8] Variable-temperature measurements were performed on the solids (**1**, **2**) by using a vibrating-sample magnetometer as described elsewhere.[9]

Crystal Structure Determination. A single crystal of **1** measuring 0.12 × 0.25 × 0.40 mm was mounted on a glass fiber and centered on a Nicolet R3m diffractometer. Cell constants and their esd's were determined by a least-squares fit of 14 diffractometer-measured reflections with $20° \le 2\theta \le 25°$. The material belongs to the monoclinic crystal class, space group *Cc*, with crystal parameters as summarized in Table I.

All intensity measurements were made at room temperature by using graphite-monochromated Mo K^α radiation (λ = 0.71069 Å) and an ω-scan technique with a variable scan rate of 3.91–29.30°/min. Background counts were taken for half the scan time at each extreme of the scan range. All data (2461) having $k, l \ge 0$ with $3° \le 2\theta \le 50°$ were measured in this manner. Crystal decomposition was monitored throughout data collection by remeasuring two standard reflections after every 50 data measurements; no significant variations were recorded. The intensities were reduced by applying Lorentz and polarization corrections. Empirical absorption corrections were applied on the basis of the azimuthal scans of suitable reflections; the maximum and minimum relative transmission values were 0.552 and 0.458, respectively. Systematic absences were eliminated to give 1164 unique data of which 1017 were considered to be observed [$|F_o| > 3\sigma(F_o)$]. All calculations were performed by using the SHELXTL package of programs.

The position of the Mn atom was determined by interpretation of a Patterson map. Initial attempts to locate the remainder of the structure in space group $C2/c$ yielded fragments of the molecule, but refinement did not proceed smoothly. The Mn atomic parameters were subsequently refined in the space group *Cc*, after which a difference Fourier map yielded all other non-hydrogen atom positions. Following refinement of the non-hydrogen atoms with anisotropic temperature factors, a difference map showed peaks at plausible hydrogen positions. The O–H hydrogen positions were fixed, and the remaining hydrogen atoms were included in ideal positions (C–H = 0.96 Å, C–C–H 120 or 109.5°). In the final cycles of blocked-cascade least-squares refinement, the non-hydrogen atoms were refined with anisotopic temperature factors and the hydrogens were varied by using a riding model. Refinement converged (shift/error ≤ 0.15) at R = 0.039, R_w = 0.045. An attempt was made to determine the absolute configuration of the helical structure by using the η-refinement technique,[10] but the results were inconclusive. All peaks of any consequence (>0.50 e/Å^3) in a final difference map were in the vicinity of the Mn atom. The quantity minimized by the least-squares program was $\sum w(|F_o| - |F_c|)^2$, where w is the weight of a given observation.[11] An extinction correction was not applied. The analytical forms

Table II. Atomic Coordinates (×10^4) and Isotropic Thermal Parameters (Å^2 × 10^3)

	x	y	z	U^a
Mn	1640 (2)	1052 (1)	1667	27 (1)
Cl(1)	2366 (2)	1042 (3)	5528 (4)	32 (1)
Cl(2)	902 (2)	1041 (4)	−1996 (5)	35 (1)
O(1)	−171 (6)	1271 (8)	2356 (14)	48 (2)
N(1)	481 (5)	1937 (10)	2211 (13)	29 (2)
C(1)	325 (4)	3101 (7)	1883 (12)	33 (2)
C(2)	1009 (7)	3947 (11)	1814 (17)	28 (2)
N(2)	1630 (8)	3288 (4)	1613 (17)	25 (1)
C(3)	954 (5)	5280 (7)	1836 (12)	38 (2)
C(4)	1607 (11)	5946 (5)	1703 (22)	37 (2)
C(5)	2281 (8)	5271 (11)	1716 (16)	32 (2)
C(6)	2303 (7)	3931 (11)	1702 (14)	24 (2)
C(7)	2956 (4)	3169 (7)	1466 (11)	33 (2)
N(3)	2811 (6)	1939 (10)	1377 (15)	35 (2)
O(2)	3431 (5)	1156 (8)	1231 (15)	48 (2)
C(8)	−465 (7)	3673 (13)	1922 (20)	58 (3)
C(9)	3717 (7)	3747 (11)	1698 (17)	42 (2)

[a] Equivalent isotropic U defined as one-third of the trace of the orthogonalized U_{ij} tensor.

Table III. Bond Lengths (Å)

Mn–Cl(1)	2.581 (3)	Mn–Cl(2)	2.468 (3)
Mn–N(1)	2.386 (10)	Mn–N(2)	2.330 (4)
Mn–N(3)	2.345 (11)	Mn–Cl(1A)	2.760 (4)
Mn–Cl(2A)	2.828 (4)	O(1)–H(1)	1.128
O(1)–N(1)	1.382 (14)	N(1)–C(1)	1.250 (13)
C(1)–C(2)	1.517 (14)	C(1)–C(8)	1.538 (15)
C(2)–N(2)	1.343 (18)	C(2)–C(3)	1.393 (14)
N(2)–C(6)	1.361 (18)	C(3)–C(4)	1.381 (19)
C(4)–C(5)	1.390 (22)	C(5)–C(6)	1.398 (16)
C(6)–C(7)	1.457 (15)	C(7)–N(3)	1.305 (12)
C(7)–C(9)	1.453 (15)	N(3)–O(2)	1.401 (14)
O(2)–H(2)	1.010		

Table IV. Bond Angles (deg)

Cl(1)–Mn–Cl(2)	178.0 (2)	Cl(1)–Mn–N(1)	92.9 (2)
Cl(2)–Mn–N(1)	85.5 (2)	Cl(1)–Mn–N(2)	91.1 (3)
Cl(2)–Mn–N(2)	89.4 (3)	N(1)–Mn–N(2)	67.2 (5)
Cl(1)–Mn–N(3)	83.4 (3)	Cl(2)–Mn–N(3)	98.6 (3)
N(1)–Mn–N(3)	133.8 (4)	N(2)–Mn–N(3)	66.9 (5)
Cl(1)–Mn–Cl(1A)	98.2 (1)	Cl(2)–Mn–Cl(1A)	82.6 (1)
N(1)–Mn–Cl(1A)	147.8 (3)	N(2)–Mn–Cl(1A)	142.0 (4)
N(3)–Mn–Cl(1A)	77.7 (3)	Cl(1)–Mn–Cl(2A)	79.3 (1)
Cl(2)–Mn–Cl(2A)	99.1 (1)	N(1)–Mn–Cl(2A)	75.3 (3)
N(2)–Mn–Cl(2A)	140.7 (4)	N(3)–Mn–Cl(2A)	147.0 (3)
Mn–Cl(1)–Mn(A)	98.6 (1)	Mn–Cl(2)–Mn(B)	99.5 (1)
N(1)–O(1)–H(1)	100.0	Mn–N(1)–O(1)	126.9 (7)
Mn–N(1)–C(1)	120.4 (7)	O(1)–N(1)–C(1)	110.5 (9)
N(1)–C(1)–C(2)	115.4 (8)	N(1)–C(1)–C(8)	122.1 (9)
C(2)–C(1)–C(8)	121.7 (8)	C(1)–C(2)–N(2)	113.5 (9)
C(1)–C(2)–C(3)	121.3 (10)	N(2)–C(2)–C(3)	125.0 (11)
Mn–N(2)–C(2)	120.9 (9)	Mn–N(2)–C(6)	119.3 (9)
C(2)–N(2)–C(6)	119.1 (8)	C(2)–C(3)–C(4)	115.9 (9)
C(3)–C(4)–C(5)	119.3 (7)	C(4)–C(5)–C(6)	122.1 (12)
N(2)–C(6)–C(5)	117.8 (11)	N(2)–C(6)–C(7)	116.7 (9)
C(5)–C(6)–C(7)	124.8 (11)	C(6)–C(7)–N(3)	112.7 (9)
C(6)–C(7)–C(9)	121.0 (8)	N(3)–C(7)–C(9)	125.4 (9)
Mn–N(3)–C(7)	123.5 (8)	Mn–N(3)–O(2)	121.1 (7)
C(7)–N(3)–O(2)	115.2 (9)	N(3)–O(2)–H(2)	104.7

(8) Evans, D. F. *J. Chem. Soc.* **1959**, 2003.
(9) Christou, G.; Collison, D.; Garner, C. D.; Acott, S. R.; Mabbs, F. E.; Petrouleas, V. *J. Chem. Soc., Dalton Trans.* **1982**, 1575.
(10) Rogers, D. *Acta Crystallogr.* **1981**, *A37*, 734–41.
(11) $w^{-1} = \alpha^2(|F_o|) + g|F_o|^2$. Final value of g = 0.00029. $R = \sum'||F_o| - |F_c||/\sum|F_o|$. $R_w = \sum[w(|F_o| - |F_c|)^2]^{1/2}/\sum(w|F_o|^2)^{1/2}$.

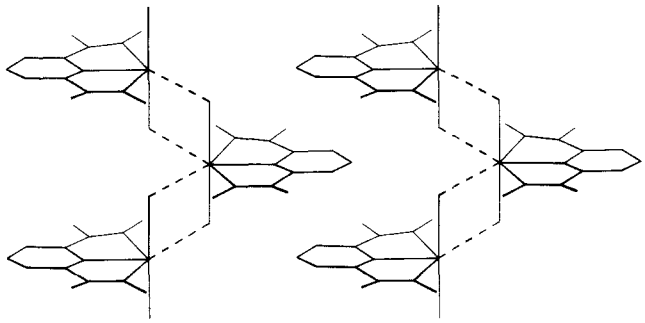

Figure 2. View of two chains as in Figure 1, showing the intercalation of the chains.

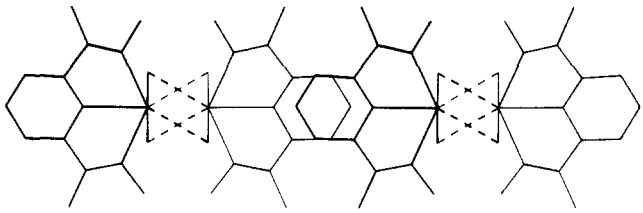

Figure 3. View down the *c* axis, showing the interaction of pyridine rings in adjacent chains.

for the scattering factors of the neutral atoms were used.[12]

Results

X-ray Crystallography. **1** crystallizes in the form of a helical polymer with $LMnCl_2$ repeating units, as shown in Figure 1. This structure is deduced from the atomic coordinates and isotropic thermal parameters (Table II). The most important bond lengths and bond angles are given in Tables III and IV, respectively. Structure factors and anisotropic thermal parameters are included in the supplementary material.

This structure is unusual because the Mn(II) is seven-coordinate, with $(N_3Cl_2)Cl_2'$ pentagonal-bipyramidal geometry around each Mn atom. The diacetylpyridine dioxime binds to Mn as a planar, tridentate ligand with three N atoms at roughly equal bond lengths to form two five-membered rings. The N(3)–Mn–N(1) angle is 133.8°, sufficiently close to twice the internal angle for a regular pentagon (2 × 72°) to accommodate two chlorine atoms in the same plane, with an average bond length of 2.80 Å. This is significantly larger than the 2.47 and 2.58 Å observed for the bond lengths involving the two axial chlorine atoms. The two axial Cl atoms define an angle with the Mn that is 178°, very close to the pure axial limit of 180°. Each of the two Cl atoms forms μ_2-bridges to two different Mn ions lying above and below the plane of the initial Mn unit. This defines two Mn_2Cl_2 parallelograms (2.5 Å × 2.7 Å) with acute angles of 79–83°, as seen also in Figure 2. These planes are rotated by an angle of 77°, relative to each other, around the axial ClMnCl vector creating a helical screw axis. The plane defined by the N(1)N(2)N(3) atoms on each ligand is slightly tilted relative to the axial ClMnCl vector by about 3–4° from a true perpendicular geometry, as seen in the projection down the normal to the pyridine rings in Figure 3. The result is a lattice with layers of planar $LMnCl_2$ units linked by bridging chlorines. Each chlorine atom occupies an axial position of one Mn atom and an equatorial position of a neighboring Mn atom in the next layer. Figure 2 shows that adjacent chains interact with each other by van der Waals forces arising from contact between nearly cofacial pyridine rings separated by 3.23 ± 0.01 Å.

Infrared Spectroscopy. The IR spectrum of the free ligand exhibits multiple bands in the range 3300–3000 cm^{-1} that have been assigned to intramolecularly hydrogen-bonded hydroxyls.[7] Complexes **1** and **2** each exhibit a sharp band at 3200 cm^{-1}, which can be assigned to free ν_{OH}. The $\nu_{C=N}$ and ν_{NO} stretching vibrations in the free ligand are observed at 1572 and 962 cm^{-1}, respectively. These vibrations are shifted to higher frequencies in **1** and **2**, appearing at 1593 and 973 cm^{-1} and at 1584 and 970 cm^{-1}, respectively. This is an indication of the coordination of the neutral oxime group (C=NOH) to the metal ion.[7] **1** also shows bands at 326 and 276 cm^{-1}, which are attributable to bridging chloride modes, and a band at 376 cm^{-1}, which can be assigned to a terminal chloride mode.[13] These data are summarized in Table V.

Table V. Selected Infrared Data for **1** and **2**

freq, cm^{-1}			
H_2dapd	**1**	**2**	assgnt
3000–3300 (b)	3200 (s)	3200 (s)	OH
1572	1593	1584	C=N
962	973	970	N–O
	376		terminal Cl
	316		μ-Cl
	276		μ-Cl

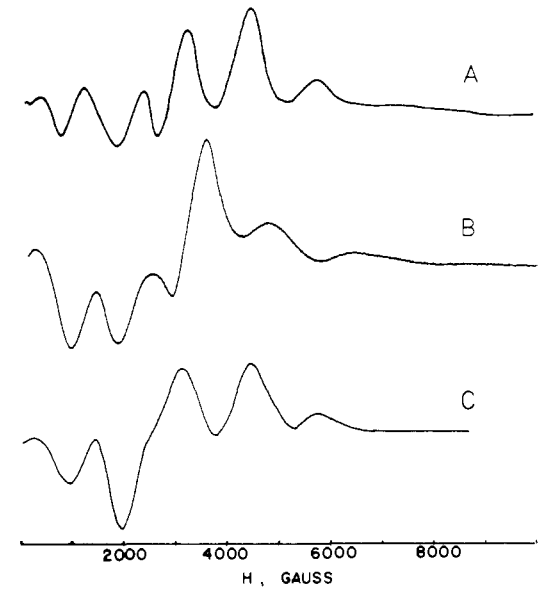

Figure 4. (A) EPR spectrum of $[Mn(H_2dapd)_2(ClO_4)_2]$ (**2**) in CH_3CN at 80 K (microwave power 110 mW; modulation amplitude 5 G; frequency 9.05 GHz). (B) EPR spectrum of $[Mn(H_2dapd)_2Br_2]$ (**3**) in CH_3CN at 110 K (microwave power 5 mW; modulation amplitude 5 G). (C) EPR spectrum of $Mn(Pz_3BH)_2$. Conditions are as in (B).

Conductivity. Complex **1** in DMF has an equivalent conductance of 28 mho cm^2 mol^{-1}, typical of a weak electrolyte. This indicates that the ligand is not ionized and so remains protonated, a result consistent with the infrared data and the low solubility in CH_3CN compared to that of **2** and **3**. On the other hand, **2** exhibits an equivalent conductance of 127.6 mho cm^2 mol^{-1}, which indicates that this is a 2:1 electrolyte, in agreement with values of 65–90 mho cm^2 mol^{-1} observed for nonassociating 1:1 electrolytes like tetrabutylammonium perchlorate and 130–170 mho cm^2 mol^{-1} for 2:1 electrolytes.[14]

EPR Spectroscopy. The X-band EPR spectra of the bromo and perchlorate derivatives **3** and **2** in CH_3CN are given in Figure 4A,B, respectively. These spectra exhibit prominent fine-structure splittings and no resolved hyperfine structure from ^{55}Mn. The temperature dependence (not shown) indicates an isolated paramagnetic ground state and slow relaxation typical of Mn(II) compounds. The fine structure is compared with that observed for the trigonally distorted six-coordinate Mn(II) complex derived from the tridentate ligand hydrotris(1-pyrazolyl)borate, $Mn^{II}(Pz_3BH)_2$ (Figure 4C). The similarity of the fine structure and temperature dependence for all three complexes indicates that these behave as electronically isolated manganese sites of D_{3h}

(12) *International Tables of X-ray Crystallography*; Kynoch Press: Birmingham, England, 1975; Vol. IV, pp 99, 149.

(13) Frank, C. W.; Rogers, L. B. *Inorg. Phys. Theor.* **1966**, *5*, 615.
(14) Geary, W. J. *Coord. Chem. Rev.* **1971**, *7*, 81.

Table VI. Summary of Electronic and Magnetic Parameters

complex	ground-state spin	$\|D\|$, cm^{-1}	A, cm^{-1}	g	J,[a] cm^{-1}
$[Mn(H_2dapd)_2Br_2]$ (**3**)	$^5/_2$	0.3	nd	nd	~0
$[Mn(H_2dapd)_2(ClO_4)_2]$ (**2**)	$^5/_2$	0.3	nd	nd	~0
$[Mn(H_2dapd)Cl_2]_n$ ($n \rightarrow \infty$) (**1**)	$5n/2$	0.1–0.2	$(6.8 \pm 0.2) \times 10^{-3}$	2	+0.2

[a] J values for the solid samples are calculated by using Fisher's formula (eq 1) with $S = {}^5/_2$. In the case of **1**, these values are approximated by ignoring zero-field splitting.

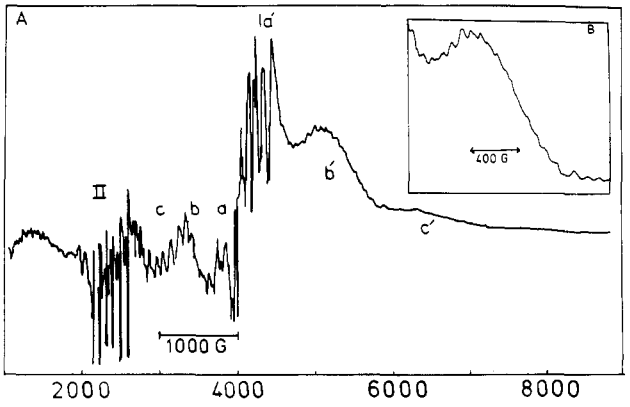

Figure 5. (A) EPR spectrum of $Mn_4(H_2dapd)_4Cl_8$ (**1**) in DMF at 10 K (microwave power 5 mW; modulation amplitude 5 G; frequency 9.24 GHz). (B) Blowup of spectrum of **1** from 3000–7000 G under identical conditions.

symmetry or lower. The positions of the fine-structure peaks indicate that the Zeeman and zero-field terms are comparable, $g\beta H \sim D \sim 0.3$ cm^{-1}.[15]

The EPR spectrum of **1** in the solid state at 77 K is a broad featureless spectrum, as expected for a weakly coupled chain of Mn(II) ions. In solution however the spectrum is much more informative and is also very different from that for the monomeric cations of **2** and **3** in solution. Two major groups of fine-structure peaks have been observed, depending upon the solvent used. In protic solvents such as alcohols and water as well as acetone, **1** breaks up into monomeric Mn(II) units that can be identified by the characteristic pattern of six ^{55}Mn hyperfine peaks. A typical hyperfine constant of 80–85 G is observed in frozen solutions. In dry DMF the spectrum given in Figure 5A is observed at 10 K. The spectrum exhibits two main groupings of transitions designated Ia–d and II. The former of these can be attributed to the zero-field splitting produced by the dipole–dipole interaction between neighboring spin $S = {}^5/_2$ ions in a cluster of Mn(II) ions. The spectrum corresponds closely to the allowed $\Delta M_S = \pm 1$ transitions observed for dimanganese(II) complexes having integral electron spin $S \geq 2$.[16] The group of peaks designated II in Figure 5A is comprised of six hyperfine peaks (average splitting 71 G) centered at an apparent g value of 4.8. The position of this group is compatible with an assignment to the double quantum transitions $\Delta M_S = \pm 2$.[16] If this assignment is correct, then the unusually large intensity of this group of lines suggests that the superexchange coupling interaction (J) between the Mn(II) ions is comparable to the zero-field splitting $D \sim 0.1$–0.3 cm^{-1}. This is also compatible with the strong temperature dependence of the spectrum (data not shown).

Ideally it is possible to determine the nuclearity of superexchange-coupled clusters of paramagnetic Mn ions from the ^{55}Mn hyperfine pattern.[17] For strongly coupled systems ($J > D$) the number of hyperfine transitions increases and the coupling constant decreases with cluster size in a predictable manner. In contrast to this situtation an irregular hyperfine pattern is observed on the various zero-field-split peaks in Figure 5A, which cannot be interpreted by using the simple models that work so well with strongly coupled clusters. Figure 5B gives a blowup of the fine-structure peak Ib', showing one region of this hyperfine structure. The average separation between peaks is 75 G, close to the range for monomeric Mn(II) complexes, but there are also many more peaks than typical for a monomeric complex. This complexity is expected for situations where the superexchange coupling is weak compared to the other magnetic interactions in the cluster; then the nuclear spins are no longer aligned by the net electronic spin vector. A summary of the magnetic and electronic parameters for compounds **1**–**3** is given in Table VI.

In conclusion, the complexity and resolution of the hyperfine pattern in combination with the zero-field splitting indicates that dissociation of **1** occurs in DMF to form a discrete oligomer rather than a heterogeneous mixture; however, the nuclearity of this oligomer cannot be uniquely determined by the EPR data owing to the extremely weak coupling between the Mn(II) ions.

Table VII. Effective Magnetic Moment at Several Temperatures

	μ_{eff}/Mn, μ_B			μ_{eff}/Mn, μ_B	
T, K	**1**	**2**	T, K	**1**	**2**
294	6.02	5.94	10.0	7.1	6.00
219	6.10	6.10	4.20	8.40	5.81
65	6.34	6.13			

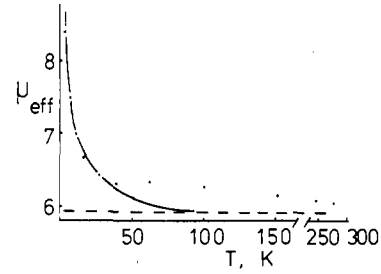

Figure 6. Experimental μ_{eff} plotted vs T for polycrystalline **1** (points). The solid curve is the theoretical prediction from Fisher's formula (eq 1) with $T_0 = 5$ K. The dashed curve is the spin-only value for an isolated high-spin Mn(II).

Magnetic Susceptibility. The effective magnetic moment (μ_{eff}/Mn) of **2** at room temperature in DMF was found to be 5.99 μ_B/Mn. This result is close to the spin-only value for an isolated Mn(II), $\mu_s = 5.92$ μ_B.

Magnetic susceptibility measurements on the powdered solids of **1** and **2** were carried out between 4.18 and 294 K and at magnetic fields up to 20 kG. μ_{eff} values for both **1** and **2** at selected temperatures are given in Table VII. For **2** a value of 5.94 μ_B at 294 K is observed, which increases by 3% to 6.13 μ_B at 65 K and then decreases by 5% to 5.80 μ_B at 4.2 K. The behavior is essentially typical of an isolated $S = {}^5/_2$ spin-only paramagnet, with weak zero-field splitting responsible for the small decrease in the limit of $T \rightarrow 0$. The weak temperature dependence indicates little or no intermolecular coupling. This is consistent with the other results establishing the perchlorate derivative to be essentially a monomeric dication $Mn(H_2dapd)_2^{2+}$ both in solution and in the solid state.

μ_{eff} for **1** behaves quite differently. Starting from a value of 6.02 μ_B at 294 K, it increases by 5% to 6.34 μ_B at 65 K. Below 35 K it increases sharply by 35% to 8.40 μ_B at 4.2 K.

A plot of μ_{eff} vs temperature for **1** is given in Figure 6. This is compared to the predicted behavior for an infinite linear chain of magnetically coupled classical spins scaled to a real spin of $^5/_2$, based upon Fisher's formula:[18]

(15) Dowsing, R. D.; Gibson, J. F. *J. Chem. Phys.* **1969**, *50*, 294.
(16) (a) Mathur, P.; Dismukes, G. C. *J. Am. Chem. Soc.* **1983**, *105*, 7093–8. (b) Mathur, P.; Crowder, M.; Dismukes, G. C. *J. Am. Chem. Soc.* **1987**, *109*, 5227.
(17) Dismukes, G. C.; Ferris, K.; Watnick, P. *Photobiochem. Photobiophys.* **1982**, *3*, 243–256.

$$\chi_M = \frac{Ng^2\mu_B^2 S(S+1)}{3kT}\,\frac{1-X}{1+X}$$
$$\mu_{eff} = \left(\frac{3k}{N\mu_\beta^2}\right)^{1/2}(\chi T)^{1/2} \qquad (1)$$

where $X = T/T_0 - \coth(T_0/T)$, with $T_0 = 2JS(S+1)/k$. T_0 is an effective spin-exchange temperature. The comparison in Figure 6 is made for the parameter $T_0 = 5$ K ($J = 0.2$ cm^{-1}, assuming $S = {}^5/_2$). The qualitative prediction of a sharply increasing magnetic moment below the coupling temperature T_0 is a feature of linear-chain ferromagnets, which these data conform to approximately. The agreement is not quantitative, possibly because of the omission of zero-field anisotropy or because of the limitations of the classical approach. Above 50 K μ_{eff} approaches the spin-only value of 5.92 μ_B shown by the dashed line. The deviation from this value is within the 5% error of the experimental measurements.

Discussion

When H_2dapd and Mn(II) salts are combined with ethanol, two entirely different compounds are formed, depending on the nature of the counterion. When Br^- or ClO_4^- is used, simple 2:1 chelates are formed, compounds **2** and **3**, respectively. This occurs even in the presence of excess Mn(II) salt. The proposed cationic structure **4** is confirmed by elemental analysis, by infrared

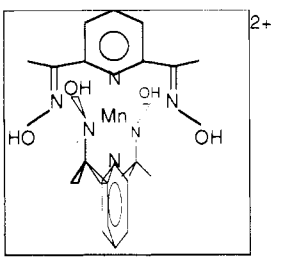

4

spectroscopy, which shows Mn coordination to N, and by EPR and magnetic susceptibility measurements, which give results typical for distorted octahedral Mn(II) mononuclear complexes. The ready solubility in solvents such as CH_3CN and high electrical conductivity are also typical of ionic coordination complexes such as **4**.

The structure of compound **1** is radically different from that of **2** and **3**. The large contraction of the N(1)–Mn–N(3) angle below 180° leaves too big a gap to be satisfied by only one additional ligand. Therefore, the monomeric $LMnCl_2$ structural unit polymerizes to form a bridged species with seven-coordinate Mn. This polymeric structure explains the low solubility in moderately polar solvents and the low conductivity in more strongly coordinating solvents such as DMF and DMSO. We have not been able to crystallize the oligomeric species observed by EPR spectroscopy in DMF solutions of **1**, so we can only speculate as to its structure. The highly resolved EPR spectrum observed in dry solvents supports formation of a single discrete cluster rather than a distribution of fragments. This changes when water is present favoring broader unresolved lines that ultimately collapse to the six-line "hexaquo" spectrum in excess water. Plausible structures for this cluster include the simple dimeric fragment of **1** $(DMF)_2LMnCl_2MnL(DMF)_2$ and tetrameric units based on the composition $(LMnCl_2)_4$. The former dimer could be envisaged as forming by partial dissolution of **1** (Figure 1) through loss of an axial and an equatorial Cl^- ligand on adjacent Mn ions while retaining the bis(μ_2-chloro)dimanganese bridge. The possible tetrameric units to consider are the linear or cyclic core Mn_4Cl_4 having alternating Mn–Cl bonds and four terminal Cl ligands or the distorted cubane cores of symmetry D_{2d} having μ_3-chloro bridges and either of the stereochemistries given by **5** or **6**. For

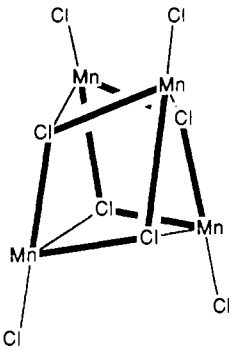

5

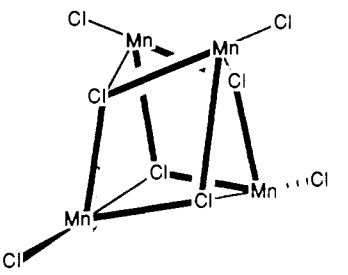

6

simplicity the H_2dapd ligands are not shown. Replacement of the terminal Cl ligands by DMF could explain the solubility in this solvent while there is retainment of the oligomeric structures. Structures **5** and **6** preserve similar bond angles as found in the solid **1** and so are compatible with the observed coordination chemistry.

There is precedent for formation of $Mn_4X_4^{4+}$ cubane cores for Mn(II) ions. The $Mn_4F_4^{4+}$ cubane core has been found to be stable in aqueous solutions. It assembles spontaneously in the presence of 5-methylpyrazole to yield a complex $Mn_4F_4L_{12}$ having three μ_3-F bridges and three terminal pyrazoles per Mn.[19] Examples of distorted cubes like **5** and **6** have also been observed for manganese(II) alkoxide clusters having cores $Mn_4(OR)_4$. A structure analogous to **5** is obtained with the bidentate ligand (hydroxymethyl)pyrazole,[20] while a macrocyclic Schiff-base ligand (derived from the 4 × 4 Schiff-base condensation of 2,6-diacetylpyridine and 1,3-diamino-2-hydroxypropane) yields a structure analogous to **6**.[21] In the latter example, the macrocycle imposes nearly pentagonal-bipyramidal site symmetry to each Mn(II) ion. This is also the site symmetry found in **1**. While precedent exists for the stability of the $Mn_4X_4^{4+}$ cubane core in solution for both halide and alkoxide bridging ligands, it may not necessarily describe the cluster that forms upon dissolution of **1** in DMF or DMSO.

Relationship to the Chloride Requirement for Photosynthetic Water Oxidation. There is a curious requirement for a small monoanion of optimum size, normally chloride, for functioning of the water-oxidizing enzyme in photosynthetic organisms.[22] Two Cl^- sites are known, and both are essential for photooxidation of the catalytic manganese site, but for different oxidation intermediates.[23,24]

EXAFS[25] and EPR[26] evidence for the Mn site have been interpreted to indicate that a large number of Cl ligands cannot be involved in the first coordination sphere of Mn. However, a small fraction of the approximately 24 donor atoms anticipated as ligands to the 4 essential Mn ions cannot be excluded as possible Cl binding sites by the present data. Also, it is known that both Cl^- removal[24] and F^- replacement[27] produce a change in the normal $g = 2$ manganese multiline EPR signal, seen in the S_2 state and attributed to a $S = {}^1/_2$ state of the Mn cluster, to a new signal at $g = 4.1$,[27,28] attributed to a $S = {}^3/_2$ state of the same cluster[29]

(18) Carlin, R. L., van Duyneveldt, A. J. In *Magnetic Properties of Transition Metal Compounds*; Springer-Verlag: New York; p 149.
(19) Ten Hoedt, R. W. M.; Reedijk, J. *Inorg. Chim. Acta* **1981**, *51*, 23.
(20) (a) Papp, F.; Bouwman, E.; Driessen, W. L.; DeGraaff, R. A. G.; Reedijk, J. *J. Chem. Soc., Dalton Trans.* **1985**, 737. (b) *Proc. Int. Conf. Coord. Chem., 14th* **1986**, 762.
(21) McKee, V.; Sheppard, W. B. *J. Chem. Soc., Chem. Commun.* **1985**, 158.
(22) Critchley, C. *Biochim. Biophys. Acta* **1985**, *811*, 33.
(23) Damoder, R.; Klimov, V. V.; Dismukes, G. C. *Biochem. Biophys. Acta* **1986**, *848*, 378.
(24) Ono, T.; Zimmerman, J.-L.; Inoue, Y.; Rutherford, A. W. *Biochim. Biophys. Acta* **1986**, *851*, 193.
(25) Yachandra, V. K.; Guiles, R. D.; McDermott, A.; Britt, R. D.; Dexheimer, S. C.; Sauer, K.; Klein, M. P. *Biochim. Biophys. Acta* **1986**, *850*, 333.
(26) Yachandra, V. K.; Guiles, R. D.; Sauer, K.; Klein, M. P. *Biochim. Biophys. Acta* **1986**, *850*, 333.
(27) Casey, J.; Sauer, K. *Biochim. Biophys. Acta* **1984**, *767*, 21.
(28) Zimmermann, J.-L.; Rutherford, A. W. *Biochemistry* **1986**, *25*, 4609.

or to an isolated Mn(III) ion.[30] These spin-state changes indicate structural changes of the Mn coordination sphere, which presumably bring about altered magnetic coupling between Mn ions in the cluster. A chloride requirement has also been noted for photoactivation of the disassembled Mn cluster, a process by which all four dissociated Mn(II) ions and Cl^- can rebind to the depleted protein complex to restore water oxidation.[31] If only Mn rebinding is assayed, an anion requirement is also observed.[32] Both the disassembly[33,34] and the reassembly of the Mn cluster indicate cooperative processes most likely associated with a discrete Mn cluster of 3-4 coupled Mn ions.

The present study has shown that depending on the nature of the counterion in solution, Mn(II) chelates with H_2dapd can assemble into monomeric Mn bis chelate complexes with noncoordinating counterions such as Br^- and ClO_4^-, while Cl^- induces assembly into an oligormic, probably dimeric or tetrameric, complex in solution. The special capability of Cl^- to serve as a bridging ligand between Mn(II) ions is thus established. Other factors are clearly important, such as the solvent and Mn oxidation state, both of which are different for the functional photosynthetic Mn site. A role for Cl^- in the initial assembly of the Mn cluster can be speculated with some justification now.

Acknowledgment. This work was supported by a grant from the National Science Foundation (CHE 82-17920) (G.C.D.) and a Research Corp. Cottrell Award (J.E.S.). Travel support from NATO Grant 236.83 is gratefully acknowledged.

Supplementary Material Available: Tables SI, SII, SIV, and SV, listing H atom coordinates and isotropic thermal parameters, anisotropic thermal parameters, independent magnetic susceptibility data, and isothermal susceptibility data for **1**, respectively (3 pages); Table III, listing observed and calculated structure factors for **1** (6 pages). Ordering information is given on any current masthead page.

(29) dePaula, J. C.; Beck, W. F.; Brudvig, G. W. *J. Am. Chem. Soc.* **1986**, *108*, 4002.
(30) Hansson, O.; Aasa, R.; Vanngard, T. *Biophys. J.* **1987**, *51*, 825.
(31) Tamura, N.; Cheniae, G. *Biochim. Biophys. Acta* **1987**, *890*, 179.
(32) Hsu, B.-D.; Lee, J.-Y.; Pan, R.-L. *Biochem. Biophys. Acta* **1987**, *890*, 89.
(33) Hunziker, D.; Abramowicz, D.; Damoder, R.; Dismukes, G. C. *Biochim. Biophys. Acta* **1986**, *890*, 6.
(34) Sivaraja, M.; Hunziker, D.; Dismukes, G. C. *Biochim. Biophys. Acta* **1988**, *936*, 228.

Contribution from the Department of Chemistry, Rensselaer Polytechnic Institute, Troy, New York 12180-3590, and Sterling Winthrop Research Institute, Rensselaer, New York 12144

Synthesis and Crystal Structure of [Ni(hMedbtaa)][TCNQ]. A Mixed-Stack Donor-Acceptor Molecular Solid

Peter J. Spellane,*[1a] Leonard V. Interrante,*[1b] Rudolph K. Kullnig,[1c] and Fook S. Tham[1b]

Received September 29, 1988

A donor-acceptor molecular solid with formula [Ni(hMedbtaa)][TCNQ] (Ni(hMedbtaa) = (hexamethyldibenzotetraazaannulenato)nickel(II); TCNQ = tetracyanoquinodimethane) was obtained on mixing methylene chloride solutions of the neutral reagent compounds. The structure consists of integrated stacks (along *a*) of planar donor macrocycles and acceptor molecules. The distance between the centers of the nonparallel donor and acceptor molecules within these stacks is half the *a*-axis dimension, or 3.99 Å. Donor and acceptor molecules also alternate along axes parallel to the *b* axis, forming a two-dimensional donor-acceptor array parallel to the (110) plane. The intramolecular bond distances and the physical properties of this compound indicate a non-charge-transferred ground state. Crystal data: $C_{36}H_{30}N_8Ni$, monoclinic, space group $P2_1/a$ (No. 14), a = 7.975 (1) Å, b = 21.845 (5) Å, c = 8.683 (1) Å, β = 98.95 (1)°, V = 1494.3 (5) Å^3, Z = 2, D_{calc} = 1.41 g/cm^3.

The electrical properties of π-donor-acceptor compounds, molecular solids that result from the interaction of planar molecular donor (D) and electron-acceptor (A) species, have been investigated for nearly 30 years.[2-5] Overlap of the molecular π-orbital systems in the stacks of donor and acceptor species that typically occur in these solids, along with, in some situations, intermolecular charge transfer, makes possible cooperative electronic or magnetic phenomena.

For example, in the prototypical "organic metal" [TTF]-[TCNQ], segregated stacks of planar tetrathiafulvalene and tetracyanoquinodimethane form, through intermolecular charge transfer, partially occupied, electronic bands, which enable high, anisotropic electronic conductivity.[6] While most of the work in the development of charge-transfer solids has involved organic molecules as both donor and acceptor species, transition-metal complexes have been used successfully as acceptor,[7] donor,[8] and both acceptor and donor[9] in the preparation of two-component π-D-A compounds. Indeed, a molecular solid formed with transition-metal complexes may have properties that derive from cooperative interactions of electrons in metal-centered orbitals as well as from interactions of ligand π-electronic systems. The planar tetraaza[14]annulene transition-metal complexes (Figure 1), having both kinds of electronic systems, can function as donor species. Redox potentials of these macrocyclic metal complexes may be tuned through substitution of peripheral hydrogen atoms or variation of the metal center. Cutler, Alleyne, and Dolphin[10] found improved solubility and ease of preparation in various methyl-substituted dibenzo macrocycles, formed from diaminobenzenes and propyl diacetals in metal template reactions. Hunziker[11-13] and others[14-16] have reported the structures and properties of several highly conductive, nonstoichiometric compounds in which substituted dibenzotetraaza[14]annulene (dbtaa)

(1) (a) Current address: IBM T. J. Watson Research Center, Yorktown Heights, NY 10598. (b) Rensselaer Polytechnic Institute. (c) Sterling Winthrop Research Institute.
(2) Simon, J.; Andre, J. J. *Molecular Semiconductors*; Springer-Verlag: New York, 1985.
(3) Epstein, A. J.; Miller, J. S. *Sci. Am.* **1979**, *240*, 52.
(4) Bechgaard, K.; Jerome, D. *Sci. Am.* **1982**, *247*, 52.
(5) Miller, J. S., Ed. *Extended Linear Chain Compounds*; Plenum: New York, 1982, 1983; Vols. 1-3.
(6) Hatfield, W. E., Ed. *Molecular Metals*: Plenum: New York, 1979.
(7) Bousseau, M.; Valade, L.; Legros, J.-P.; Cassoux, P.; Garbauskas, M.; Interrante, L. *J. Am. Chem. Soc.* **1986**, *108*, 1908. Bousseau, M.; Valade, L.; Bruniquel, M.-F.; Cassoux, P.; Garbauskas, M.; Interrante, L.; Kasper, J. *Nouv. J. Chim.* **1984**, *8*, 3.
(8) Endres, H.; Bongart, A.; Nothe, D.; Hennig, I.; Schweitzer, D.; Schafer, H.; Helberg, H.; Flandrois, S. *Z. Naturforsch.* **1985**, *40B*, 489.
(9) Cassoux, P.; Interrante, L.; Kasper, J. *Mol. Cryst. Liq. Cryst.* **1982**, *81*, 293. See also: Interrante, L. V.; Browall, K. W.; Hart, H. R.; Jacobs, I. S.; Watkins, G. D.; Wee, S. H. *J. Am. Chem. Soc.* **1975**, *97*, 889. Interrante, L. V.; Secaur, C. A. *J. Am. Chem. Soc.* **1975**, *97*, 890. Interrante, L. V. *Adv. Chem. Ser.* **1976**, *No. 150*, 1.
(10) Cutler, A. R.; Alleyne, C. S.; Dolphin, D. *Inorg. Chem.* **1985**, *24*, 2276.
(11) Hunziker, M.; Hilti, B.; Rihs, G. *Helv. Chim. Acta* **1981**, *64*, 82.
(12) Hunziker, M.; Loeliger, H.; Rihs, G.; Hilti, B. *Helv. Chim. Acta* **1981**, *64*, 2544.
(13) Hunziker, M.; Rihs, G. *Inorg. Chim. Acta* **1985**, *102*, 39.
(14) Lin, L.-S.; Marks, T.; Kannewurf, C.; Lyding, J.; McClure, M.; Ratajack, M.; Whang, T.-C. *J. Chem. Soc.* **1980**, 954.
(15) Hatfield, W. E. *Polym. Sci. Technol.* **1981**, *15*, 57.
(16) Wu, Y.-M.; Peng, S.-M.; Chang, H. *J. Inorg. Nucl. Chem.* **1980**, *42*, 839.

0020-1669/89/1328-1587$01.50/0 © 1989 American Chemical Society